Uncovering the matter-neutrino resonance

D. Väänänen and G. C. McLaughlin

Phys. Rev. D **93**, 105044 — Published 26 May 2016

DOI: 10.1103/PhysRevD.93.105044

Uncovering the Matter-Neutrino Resonance

D. Väänänen[1] and G. C. McLaughlin[1]

[1]*Department of Physics, North Carolina State University, Raleigh, NC 27695 USA.*

Matter Neutrino Resonances (MNRs) can drastically modify neutrino flavor evolution in astrophysical environments and may significantly impact nucleosynthesis. Here we further investigate the underlying physics of MNR type flavor transitions. We provide generalized resonance conditions and make analytical predictions for the behavior of the system. We discuss the adiabatic evolution of these transitions considering both Symmetric and Standard MNR scenarios. *Symmetric* MNR transitions differ from *Standard* MNR transitions in that both neutrinos and antineutrinos can completely transform to other flavors simultaneously. We provide an example of the simplest system in which such transitions can occur with a neutrino and an antineutrino having a single energy and emission angle. We further apply linearized stability analysis to predict the location of self-induced nutation type (or bipolar) oscillations due to $\nu\nu$ – interactions in the regions where MNR is ineffective. In all cases, we compare our analytical predictions to numerical calculations.

PACS numbers: 14.60.Pq1,97.60.Jd,3.15.+g
Keywords: neutrino mixing, neutrinos-neutrino interaction

I. INTRODUCTION

Compact object mergers and core collapse supernovae release a significant fraction of their energy in the form of neutrinos, e.g. [1–7]. These neutrinos play a number of roles, for example they are a key player in determining the types of nucleosynthesis that come from the winds in these objects, e.g. [8, 9]. Developing further understanding of neutrino flavor evolution in these environments is necessary for gaining a complete picture of the nature of neutrino evolution in astrophysical settings. In addition, an understanding of the flavor content of the neutrino spectrum is essential for determining whether the suitable conditions for the synthesis of various types of heavy elements can be met, e.g. [10, 11] as well as for extracting the most information from future observations.

Neutrino flavor evolution in dense astrophysical environments is inherently a complex quantum many-body problem [12–20]. Neutrinos are known to be able to transform from one type to another as they propagate freely in space. Interactions with the particles in the surrounding environment can drastically modify their flavor evolution with significant consequences. The MSW resonance conversion effect is known to be responsible for the neutrino transitions in the Sun, solving the long standing solar neutrino problem [21–24]. Neutrino interactions with other surrounding neutrinos can become important in environments with extremely high neutrino densities, such as in supernovae or in accretion disks above merging compact objects. In these environments, neutrino-neutrino potential can induce collective nutation type flavor transformation effects distinct from the MSW effect [25–27]. At the highest densities, the quantum many-body nature of the problem can break several commonly utilized assumptions leading to a possibility of novel effects [17, 18, 20, 28–31].

In this manuscript, we concentrate on a new type of neutrino flavor transformation effect which was observed in the recent simulations of neutrino flavor evolution above black hole accretion disks [11]. Accretion disks produce mostly electron type neutrinos and antineutrinos. Antineutrinos have smaller emission disks with respect to neutrinos but are emitted with a hotter spectrum than that of neutrinos. Therefore, close to the neutrino emission disk antineutrino flux can dominate over neutrino flux. This is a distinct feature compared to standard proto-neutron star supernova neutrino scenarios.

In Ref. [11], two new types of neutrino transformations were observed which differ from the known MSW resonance and the self-induced bipolar transitions. In one of these transformations neutrinos fully convert to other flavors while antineutrinos return to their original configuration. This transformation was further investigated in Ref. [32] and was understood to be a consequence of a *Matter Neutrino Resonance* (MNR) achieved by an active cancellation of the neutrino-neutrino potential and the background matter contribution. Hereafter, we refer to this type of transformation as *Standard* MNR transition. Another type of transformation that was observed in [11] fully converted both neutrinos *and* antineutrinos symmetrically. In Ref. [33] numerical studies were performed examining both Standard and Symmetric MNR and exploring their consequences for nucleosynthesis. Similar effects can occur in other non-linear systems that exhibit similar features, such as in the presence of neutrino-antineutrino spin coherence [29] or active-sterile neutrino mixing.

In order to fulfill the MNR condition, the neutrino-neutrino and the background matter potentials are required to have opposite signs. A characteristic feature of a MNR is that the system can maintain the resonance over

extended period by suitably transforming neutrinos to other flavors. We will present analytic conditions for the occurrence of MNR by deriving general resonance and adiabaticity conditions. We discuss the adiabatic evolution of the (anti)neutrino in-medium energy eigenstates. We further demonstrate that analytic expressions, that describe accurately (anti)neutrino survival probabilities during MNR transition, can be obtained by assuming the separation of the in-medium energy eigenvalues stay close throughout the transition.

In the presence of large background matter, when MNR transition occurs, the analytic expressions for the survival probabilities have only a small dependence on the vacuum mixing parameters. However, as discussed in [32] the presence of MNR transitions does depend on the values of these parameters. Furthermore, the vacuum mixing and the changing background potentials affect adiabaticity of the evolution impacting the feasibility of MNR transitions. Here we will investigate the possible effects that the interplay between the vacuum parameters and the variation of the background potentials can induce. For instance, in the absence of MNR transitions, neutrinos can undergo collective self-induced nutation type (or *bipolar*) neutrino flavor transitions.

Analytic conditions for the occurrence of self-induced effects have been obtained for two-neutrino systems with simplified (single-angle) geometrical dependence [27, 34–38]. The onset of these self-induced effects has been related to the presence of an instability. In the context of supernova neutrinos the idea of employing linearized equations was first pointed out in Ref. [39]. This idea was further developed in Ref. [40] where stability conditions were derived for the self-induced nutation type flavor transitions allowing to study conditions for the multi-emission angle effects in the case of two neutrino flavors. Thereafter, linearized stability analysis has been employed in several works, studying the suppression of collective effects during the accretion phase [41, 42], the effects of realistic emission angular distributions [43–45], the presence of spurious instabilities due to the numerical inputs [46], the effects of neutrino scattering outside the neutrinosphere [47], instabilities triggered by flavor oscillation modes [48], the effects of breaking the axial symmetry [49] and deleptonization asymmetry [50], temporal instabilities [51] and effects of small scale features [52]. General linearized equations, applicable to arbitrary number of flavors and a general form of the Hamiltonian, were derived in Ref. [18]. In this manuscript, for the first time, we will apply the linearization procedure described in Ref. [18] to systems with MNR resonances.

The manuscript is structured as follows. In Sec. II we describe the two flavor monoenergetic model as well as the density matrix formalism that we will use. In Sec. III we derive the resonance conditions and the analytical expressions for the survival probabilities, illustrating the predictive power of our results with systems that exhibit either Symmetric MNR transitions or Standard MNR transitions. We then consider systems that have MNR resonances but not MNR transitions due to the suppression associated with small mixing angles. This analysis can also be used to mimic the effects of varying background densities. In these cases, we demonstrate the usefulness of utilizing linear stability analysis to predict traditional bipolar transition regions.

II. THE SET UP

A. The Model

In the following, we will consider a system that can be described by two (anti)neutrino flavors, which are produced and emitted with a single energy and a single emission angle. Neutrinos are assumed to be produced with a specific flavor described by an interaction eigenstate (or *flavor* state) $|\nu_f\rangle$ ($f = e, \mu$ or τ)[1]. The propagation eigenstates in vacuum, $|\nu_{i,j}\rangle$ ($i, j = 1, 2$), can be written in terms of the flavor eigenstates as

$$\begin{aligned} |\nu_1\rangle &= \cos\theta_V\,|\nu_e\rangle + \sin\theta_V\,|\nu_x\rangle\ , \\ |\nu_2\rangle &= -\sin\theta_V\,|\nu_e\rangle + \cos\theta_V\,|\nu_x\rangle\ , \end{aligned} \tag{1}$$

with the vacuum mixing angle, θ_V, determining the relative proportionality of the states. We define the mass-squared splitting between the neutrino propagation eigenstates in vacuum as $\delta m^2 \equiv m_2^2 - m_1^2$. Similar equations hold for antineutrinos.

The evolution of the considered system can be described by solving the following equations of motion for neutrino,

[1] For a discussion on applicability of this assumption see e.g. Refs. [53] and references therein.

ρ, and antineutrino, $\bar{\rho}$, density matrices, respectively,[2]:

$$\mathrm{i}\frac{\mathrm{d}\rho}{\mathrm{d}r} = [H, \rho\,] \ , \quad \mathrm{i}\frac{\mathrm{d}\bar{\rho}}{\mathrm{d}r} = \left[\bar{H}, \bar{\rho}\,\right], \tag{2}$$

where r represents a distance outside the neutrino emission surface from the center of the source object. In flavor basis the neutrino and antineutrino density matrices are defined, respectively, as

$$\begin{aligned} \rho &= \begin{pmatrix} \rho_{ee} & \rho_{ex} \\ \rho_{xe} & \rho_{xx} \end{pmatrix} = \begin{pmatrix} |a_{\nu_e}|^2 & a_{\nu_e} a^*_{\nu_x} \\ a^*_{\nu_e} a_{\nu_x} & |a_{\nu_x}|^2 \end{pmatrix} \ , \\ \bar{\rho} &= \begin{pmatrix} \bar{\rho}_{ee} & \bar{\rho}_{ex} \\ \bar{\rho}_{xe} & \bar{\rho}_{xx} \end{pmatrix} = \begin{pmatrix} |a_{\bar{\nu}_e}|^2 & a_{\bar{\nu}_e} a^*_{\bar{\nu}_x} \\ a^*_{\bar{\nu}_e} a_{\bar{\nu}_x} & |a_{\bar{\nu}_x}|^2 \end{pmatrix} \ , \end{aligned} \tag{3}$$

where $a_{\nu_f^{(-)}}$ is a probability amplitude of a (anti)neutrino being in a given configuration f.

The total neutrino Hamiltonian of the investigated system in the flavor basis, H_F, consists of the vacuum, H_V, the background matter, H_e, and the neutrino-neutrino interaction, $H_{\nu\nu}$, contributions:

$$H_F = H_V + H_e + H_{\nu\nu} \ . \tag{4}$$

The vacuum Hamiltonian is given by

$$H_V = \frac{\Delta_V}{2} \begin{pmatrix} -\cos 2\theta_V & \sin 2\theta_V \\ \sin 2\theta_V & \cos 2\theta_V \end{pmatrix} \ , \tag{5}$$

where $\Delta_V \equiv \delta m^2/(2E)$ with neutrino mass-squared splitting in vacuum, δm^2, and neutrino energy, E. The background matter contribution can be written as

$$H_e = \begin{pmatrix} V_e & 0 \\ 0 & 0 \end{pmatrix}, \tag{6}$$

where $V_e = \sqrt{2} n_e$ is the electron potential arising from the difference between net electron and positron number densities $n_e = n_e^- - n_e^+$. The neutrino-neutrino interactions that couple the evolution of the neutrino and antineutrino densities are described by

$$H_{\nu\nu} = \mu_\nu \left(\rho - \alpha \bar{\rho}^*\right) \ , \tag{7}$$

with interaction strength, μ_ν[3], asymmetry factor, α, defining the relative difference between the initial ν_e and $\bar{\nu}_e$ number fluxes and * indicating complex conjugation operation. For antineutrinos the total interaction Hamiltonian is given by

$$\bar{H}_F = H_V - H_e - H^*_{\nu\nu} \ . \tag{8}$$

For a derivation of these contributions in the utilized formalism see Ref. [17].

A diagonal contribution can always be extracted from the Hamiltonian without impacting the flavor evolution described by Eqs. (2). By subtracting a common factor $1/2\left(V_e + \mu(\rho_{ee} + \rho_{xx} - \alpha(\bar{\rho}_{ee} + \bar{\rho}_{xx}))\right) \mathrm{Diag}(1,1)$ from Eq. (4), the total flavor basis neutrino Hamiltonian can be written in a symmetrized form as

$$H_F = \frac{1}{2} \begin{pmatrix} -\Delta_V \cos 2\theta_V + V_e + V_\nu & \Delta_V \sin 2\theta_V + V^{ex}_\nu \\ \Delta_V \sin 2\theta_V + V^{xe}_\nu & \Delta_V \cos 2\theta_V - (V_e + V_\nu) \end{pmatrix}, \tag{9}$$

where

$$\begin{aligned} V_\nu &\equiv \mu_\nu \left(\rho_{ee} - \rho_{xx} - \alpha(\bar{\rho}_{ee} - \bar{\rho}_{xx})\right) \ , \\ V^{ex}_\nu &\equiv 2\mu_\nu(\rho_{ex} - \alpha \bar{\rho}_{xe}) \ . \end{aligned} \tag{10}$$

The antineutrino Hamiltonian is obtained from the above expression by replacing $V_e \to -V_e$, $V_\nu \to -V_\nu$ and $V^{ex}_\nu \to -V^{xe}_\nu$.

---

[2] For a derivation and listing of underlying assumptions of the utilized approach see Ref. [17].

[3] In general, μ_ν comprises the interaction scale and momentum dependence term: $\sqrt{2} G_F \int (1 - \mathbf{p}\cdot\mathbf{q})$ with test and background neutrino momenta $\mathbf{p}$ and $\mathbf{q}$. Neutrino number flux density of a neutrino with flavor f described by density matrix, $\rho_{\mathbf{p},f}$, with momentum $\mathbf{p}$, can be written in terms of neutrino luminosity, L, and average energy, $\langle E \rangle$, as $\int \mathrm{d}^3\mathbf{p}/(2\pi)^3\, \rho_{\mathbf{p},\mathrm{f}} = \int \mathrm{dE}\, \mathrm{d}\phi\, \mathrm{d}\cos\theta\, \mathrm{L}\, \mathrm{D}(\mathrm{E},\theta,\phi)/(4\pi \mathrm{R}^2 \langle \mathrm{E} \rangle)$, with energy and angular distribution D, expressed in spherical coordinates with polar angle, θ, and azimuthal angle, ϕ.

III. RESULTS

A. Resonance and Adiabaticity Conditions

First we will derive equations to predict the location of the *Matter-Neutrino Resonance* (MNR). Then we proceed to derive equations to predict the anticipated behavior of the flavor evolution at the resonances by introducing a generalized *adiabaticity* parameter. The symmetrized flavor basis Hamiltonian, Eq. (9), can be diagonalized using a unitary $SU(2)$ rotation matrix U_M:

$$U_M^\dagger H_F U_M \equiv \frac{\Delta_M}{2}\mathrm{Diag}(-1,1) \equiv H_M \ , \tag{11}$$

where H_M is the instantaneous *in-medium* eigenbasis Hamiltonian with (anti)neutrino energy eigenstates $\pm\overset{(-)}{\Delta}_M$. The eigen-energies define the (*effective*) in-medium mass-squared splitting, δm^2_{eff}:

$$\overset{(-)}{\Delta}_M \equiv \frac{\delta m^2_{eff}}{2E} = \sqrt{\left(\Delta_V \cos 2\theta_V \overset{(+)}{-} (V_e + V_\nu)\right)^2 + \left(\Delta_V \sin 2\theta_V \overset{(-)}{+} V_\nu^{ex}\right)\left(\Delta_V \sin 2\theta_V \overset{(-)}{+} V_\nu^{xe}\right)} \quad , \tag{12}$$

with parenthesis indicating the differences in case of antineutrinos.

The most general form of the rotation matrix (or *in-medium mixing matrix*) U_M can be written as

$$U_M = \begin{pmatrix} 1 & 0 \\ 0 & \mathrm{e}^{-\mathrm{i}\delta_M} \end{pmatrix} \begin{pmatrix} \cos\theta_M & \sin\theta_M \\ -\sin\theta_M & \cos\theta_M \end{pmatrix} \begin{pmatrix} \mathrm{e}^{\mathrm{i}\beta_{1M}} & 0 \\ 0 & \mathrm{e}^{\mathrm{i}\beta_{2M}} \end{pmatrix} \ . \tag{13}$$

where θ_M is the in-medium mixing angle and $\delta_M, \beta_{1M,2M}$ are in-medium phases. The flavor composition of in-medium eigenstates, $|\nu_{iM}\rangle$ $(i = 1, 2)$, is obtained from the corresponding expression in vacuum, Eq. (1), by replacing the vacuum mixing angle, θ_V, with the in-medium angle θ_M. The flavor Hamiltonian H_F can then be written in terms of the in-medium quantities as

$$H_F = U_M H_M U_M^\dagger = \frac{\Delta_M}{2} \begin{pmatrix} -\cos 2\theta_M & \sin 2\theta_M \mathrm{e}^{\mathrm{i}\delta_M} \\ \sin 2\theta_M \mathrm{e}^{-\mathrm{i}\delta_M} & \cos 2\theta_M \end{pmatrix} \ . \tag{14}$$

Notice that this expression is independent of the β phases. The expressions for the flavor basis Hamiltonian in Eqs. (9) and (14) give the following relations for the in-medium quantities:

$$\begin{aligned} \Delta_M \cos 2\theta_M &= \Delta_V \cos 2\theta_V - (V_e + V_\nu) \ , \\ \Delta_M \sin 2\theta_M \mathrm{e}^{\mathrm{i}\delta_M} &= \Delta_V \sin 2\theta_V + V_\nu^{ex} \ . \end{aligned} \tag{15}$$

Combining the above relations one obtains the following equations for the in-medium mixing angle, θ_M, and phase, δ_M:

$$\begin{aligned} \tan 2\theta_M \mathrm{e}^{\mathrm{i}\delta_M} &= \frac{\tan 2\theta_V + \dfrac{V_\nu^{ex}}{\Delta_V \cos 2\theta_V}}{1 - \dfrac{V_e + V_\nu}{\Delta_V \cos 2\theta_V}} \ , \\ \tan\delta_M &= \mathrm{i}\ \frac{V_\nu^{ex} - V_\nu^{xe}}{2\Delta_V \sin 2\theta_V + V_\nu^{ex} + V_\nu^{xe}} = -\frac{\mathcal{I}m[V_\nu^{ex}]}{2\Delta_V \sin 2\theta_V + \mathcal{R}e[V_\nu^{ex}]} \ . \end{aligned} \tag{16}$$

The resonance condition is readily determined from above as:

$$(V_e + V_\nu)|_{r=r_R} = \Delta_V \cos 2\theta_V \ , \tag{17}$$

where R indicates that the quantities are evaluated at the resonance location $r = r_R$. This equation allows one to determine the expected location of MNR.

Neutrino flavor evolution at a resonance depends on how the resonance is crossed. We quantify the crossing behavior by defining an *adiabaticity parameter*, γ, similarly as in Ref. [37][4]:

$$\gamma \equiv \frac{|\Delta_M|}{\left|\frac{\mathrm{d}\theta_M}{\mathrm{d}r} + \mathrm{i}\frac{\sin 2\theta_M}{2}\frac{\mathrm{d}\delta_M}{\mathrm{d}r}\right|} \ , \tag{18}$$

with the in-medium mass-squared splitting, Δ_M from Eq. (12). The rate of change of the in-medium mixing is given by

$$\frac{\mathrm{d}\theta_M}{\mathrm{d}r} = \frac{\Delta_M \frac{\mathrm{d}H_{ee}}{\mathrm{d}r} - H_{ee}\frac{\mathrm{d}\Delta_M}{\mathrm{d}r}}{2\Delta_M |H_{ex}|} \ , \tag{19}$$

and the rate of change of the in-medium phase by

$$\frac{\mathrm{d}\delta_M}{\mathrm{d}r} = \frac{H_{ex}^{\mathcal{R}e}\frac{\mathrm{d}H_{ex}^{\mathcal{I}m}}{\mathrm{d}r} - H_{ex}^{\mathcal{I}m}\frac{\mathrm{d}H_{ex}^{\mathcal{R}e}}{\mathrm{d}r}}{|H_{ex}|^2} \ , \tag{20}$$

where

$$\begin{aligned} H_{ee} &= \Delta_V \cos 2\theta_V - (V_e + V_\nu) \ , \\ H_{ex} &= \Delta_V \sin 2\theta_V + V_\nu^{ex} \end{aligned} \tag{21}$$

are, respectively, the diagonal and the off-diagonal elements of the flavor basis Hamiltonian in Eq. (9) with V_ν and V_ν^{ex} given by Eq. (10)[5].

If the rate of change of the in-medium mixing is much smaller with respect to the splitting of the energy eigenstates ($\gamma > 1$), neutrino stays on its in-medium eigenstate. In this case, we refer the evolution as being completely adiabatic. At the other extreme, if neutrino jumps to the other in-medium eigenstate, the evolution is said to be completely non-adiabatic ($\gamma < 1$). The adiabaticity of the resonance crossing in our systems can be evaluated by applying expressions for the in-medium quantities in Eqs. (12) and (16) to the definition of the full adiabaticity parameter from Ref. [37]. At a location of the resonance the adiabaticity parameter becomes:

$$\gamma_R = \left.\frac{2\Delta_M^2 \sin 2\theta_M}{\left|\frac{\mathrm{d}V_e}{\mathrm{d}r} + \frac{\mathrm{d}V_\nu}{\mathrm{d}r}\right|}\right|_{r=r_R} \ . \tag{22}$$

In case of no flavor transformation, at the location of resonance Δ_M reduces to its vacuum contribution $\Delta_V \sin 2\theta_V$, such that, utilizing relation Eq. (15), in the above expression $\Delta_M^2 \sin 2\theta_M|_{r=r_R} = \Delta_V^2 \sin^2 2\theta_V$.

While the expression for the adiabaticity parameter, γ in Eq. (18), can be used to indicate whether a neutrino stays on its in-medium mass eigenstate or not, another measure of adiabaticity can be obtained by comparing the in-medium mass eigenstate to the actual state of the system. The more similar these are, the more adiabatic the system is. To make this comparison we will calculate the survival probability of the neutrinos and compare it to the projection of the in-medium mass eigenstate onto the original neutrino flavor.

If a neutrino stays on its in-medium eigenstate, one can write the probability of finding a neutrino with a flavor f from the in-medium state, $|\nu_{iM}\rangle$, as

$$P(\nu_f|\nu_{iM}) \equiv |\langle \nu_f|\nu_{iM}\rangle|^2 \ . \tag{23}$$

Again, in case of completely adiabatic evolution, the above probability should match the neutrino survival probability. Utilizing the relations in Eq. (15), the probability of finding an electron neutrino from an in-medium eigenstate $|\nu_{1M}\rangle$

---

[4] Notice that in Ref. [37] the authors defined a non-adiabaticity parameter Γ, which is the inverse of our definition: $\gamma \equiv 1/\Gamma$.

[5] The superscripts $\mathcal{R}e$ and $\mathcal{I}m$ refer to real and imaginary components of the given matrix element, respectively.

can be expressed as

$$\begin{aligned} P(\nu_e|\nu_{1M}) = |\langle\nu_e|\nu_{1M}\rangle|^2 =& \cos^2\theta_M \\ =& \frac{1}{2}\left(1 + \frac{\Delta_V \cos 2\theta_V - (V_e + V_\nu)}{\Delta_M}\right) \\ =& \frac{1}{2}\left(1 + \frac{1}{\sqrt{1 + |\tan 2\theta_M|^2}}\right) , \end{aligned} \tag{24}$$

where

$$|\tan 2\theta_M|^2 = \frac{(\Delta_V \sin 2\theta_V + V_\nu^{ex})(\Delta_V \sin 2\theta_V + V_\nu^{xe})}{(\Delta_V \cos 2\theta_V - (V_e + V_\nu))^2} , \tag{25}$$

with neutrino-neutrino interaction potential, V_ν, and the off-diagonal contribution, V_ν^{ex}, given by Eq. (10). In the next two subsections, we study adiabaticity in systems that exhibit MNR type transitions.

B. Numerical Results

In this section, we use the expressions from the previous section to solve the evolution equations by numerical integration and use the results to determine the adiabaticity of the evolution of a neutrino in a Symmetric MNR system. We illustrate our results with an example which is configured to capture the primary features and the relative scales of the symmetric MNR systems that were first seen in [11, 33]. We consider a scenario where the neutrino potential starts negative and becomes positive, with an explicit parametrization of $\mu_\nu = 10\,000\ [\Delta_V]$ and the initial ν_e and $\bar{\nu}_e$ asymmetry factor, $\alpha(r) = a + br$, with $a = 1.3$ and $b = -0.048$ with distance expressed in units of inverse vacuum scale $[\Delta_V^{-1}]$. The matter potential is assumed to be constant: $V_e = 1000\ [\Delta_V]$.

Using the above parametrization, we numerically solve the evolution equations, Eqs. (2), assuming an inverted neutrino mass hierarchy, $\Delta_V = -1$, and a vacuum mixing corresponding to the measured value of θ_{13}; $\theta_V = 0.15$. In Fig. 1, we plot the diagonal element of the neutrino density matrix in Eq. (3), corresponding to the neutrino survival probability, as the dashed red line. We also use the numerical solutions of Eqs. (2) to determine the electron flavor component of the in-medium mass eigenstate and plot the corresponding probability, Eq. (24), shown as the orange solid line in Fig. 1. Here, we can see that the numerically computed survival probability and the probability of finding an electron neutrino from the in-medium eignestate match well over long timescales. However, over a shorter timescale, we can see oscillations in the numerical in-medium state solution that do not appear in the true state as determined from the numerically computed survival probability. From this, we can infer that the system is adiabatic over long timescales and nonadiabatic over shorter timescales.

Using the numerical solutions of Eqs. (2), we also calculate the adiabaticity parameter, γ in Eq. (18), over both scales. This parameter requires information about the off-diagonal components of the density matrices in Eq. (3) which we have plotted in the bottom panel of Fig. 1. In order to compute the adiabaticity parameter, we also need to compute the derivatives in Eqs. (19) and (20). To determine the adiabaticity over the entire length of the transition we use values of the derivatives in Eqs. (19) and (20) averaged over the length of the entire transition. This procedure yields $\gamma \approx 2$. To determine the adiabaticity over the shorter timescale seen in Fig. 1, we again calculate the average derivatives, but this time over one fourth of the visible oscillation scale seen in the top panel of Fig. 1. For this smaller scale, we find that the adibaticity parameter has a significantly smaller value, $\gamma \approx 0.06$. Thus, our test for the adiabaticity using Eq. (18), predicts (barely) adiabatic behavior over long scales and non-adiabatic behavior on the shorter scale. We note that the derivative of the phase, Eq. (20), becomes larger in the smaller scale case, however, in both the larger and the smaller timescales, the derivative of the in-medium mixing angle, Eq. (19), dominates the denominator in the expression for the adiabaticity parameter, Eq. (18).

C. Analytical Expressions for the Survival Probabilities

We now consider two different analytic methods to predict the survival probability during a MNR transition. Neither of these methods use the numerical integration of the evolution equations described in the previous section. First, we demonstrate that analytical expressions for the neutrino during MNR transitions can be obtained by assuming that

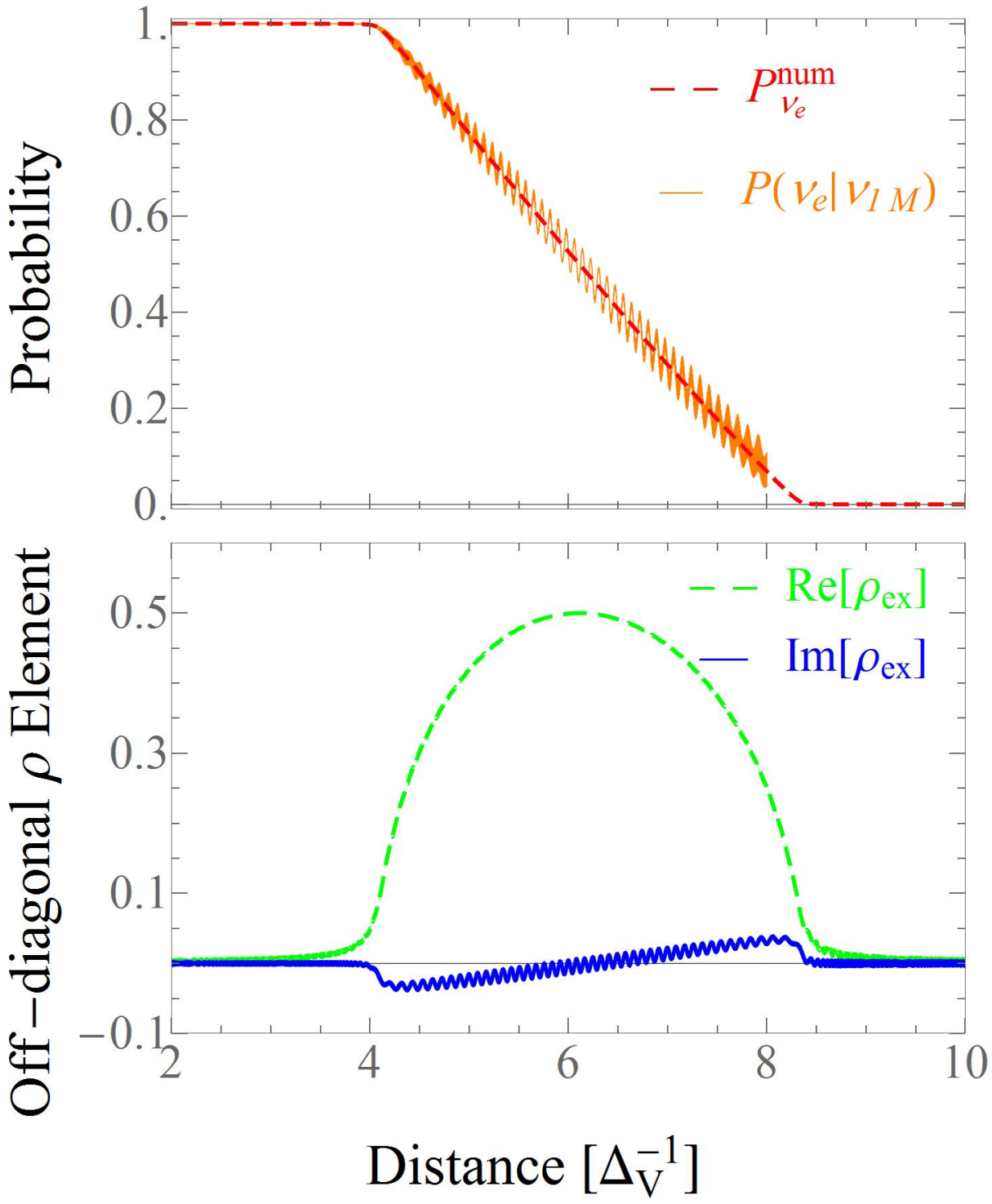

FIG. 1: (Color online) Numerical results for the elements of the neutrino density matrix obtained by numerically solving the evolution equations Eq. (2). Top figure: ν_e survival probability, P_{ν_e} (red), and a probability, $P(\nu_e|\nu_{1M})$, given by Eq. (24) (orange lines) of finding an electron neutrino from in-medium eigenstate, ν_{1M}. Bottom figure: real and imaginary components of the off-diagonal neutrino density matrix elements. Here we have considered the Symmetric MNR model (see text for details) in inverted neutrino mass hierarchy, $\Delta_V = -1$ with vacuum mixing angle $\theta_V = 0.15$.

the in-medium energy values stay close throughout the transition. Then, we show that another, similar expression

can be obtained by assuming that a neutrino remains on its in-medium eigenstate during the MNR transition. We will compare both of these probabilities with the numerical solutions presented in the previous subsection.

1. Vanishing In-medium Splitting Assumption

The separation of the in-medium neutrino energy eigenvalues defines the in-medium mass splitting, Δ_M, given by Eq. (12). Assuming that at some point during the evolution the in-medium eigenvalues become very close, this "gap" reaches its minimum when $\Delta_M \approx 0$. By inspection of Eq. (12) one obtains two conditions, one for the flavor diagonal contributions:

$$\Delta_V \cos 2\theta_V - (V_e + V_\nu) \approx 0 \ , \tag{26}$$

and another one for the flavor off-diagonal contributions:

$$\Delta_V \sin 2\theta_V + V_\nu^{ex} \approx 0 \quad (\text{or} \quad \Delta_V \sin 2\theta_V + V_\nu^{xe} \approx 0) \ . \tag{27}$$

The first condition, Eq. (26), is equivalent with the resonance condition Eq. (17).

The second condition, Eq. (27), reduces to the conditions found in Ref. [32] for the off-diagonal terms in the limit of vanishing vacuum contribution[6]. Neglecting the vacuum terms, in Ref. [32] the above conditions were used to obtain analytical expressions for the electron (anti)neutrino survival probabilities when the MNR conditions are fulfilled:

$$\begin{aligned} P_{\nu_e} \equiv \rho_{ee} &= \frac{1}{2}\left(1 + \frac{\alpha^2 - R^2 - 1}{2R}\right) \ , \\ P_{\bar{\nu}_e} \equiv \bar{\rho}_{ee} &= \frac{1}{2}\left(1 + \frac{\alpha^2 + R^2 - 1}{2\alpha R}\right) \ , \end{aligned} \tag{28}$$

where $R \equiv V_e/\mu_\nu$ is the ratio of the neutrino-electron and neutrino-neutrino interaction scales. These equations were found to be in excellent agreement with the numerical results in Ref. [32] during the MNR transition.

We compare the numerically calculated Symmetric MNR transition probability with the analytic prediction, Eq. (28) in the top left of Fig. 2 for the same Symmetric MNR system as in Fig. 1. From the figure we can see that the analytic prediction, stemming from the assumption of maintaining a small "gap" between the instantaneous eigenvalues closely tracks the numerics.

In obtaining Eq. (28) we have not assumed that the neutrino remains on an in-medium eigenstate, only that the eigenvalues come close together. However, we demonstrated numerically in the previous section that the long timescale behavior of the system can, on average, be adiabatic. Therefore, in the next section we derive an expression assuming that the state of the system remains similar to the in-medium eigenstate.

2. Adiabatic Assumption

In an adiabatic assumption, one assumes that the projected probability of finding a certain type of (anti)neutrino from a given in-medium eigenstate equals to the (anti)neutrino survival probability given by the diagonal element of the (anti)neutrino density matrix. Rewriting Eq. (24), we find

$$\rho_{ee} = P_{\nu_e} \approx P(\nu_e|\nu_{1M}) = \frac{1}{2}\left(1 + \frac{\Delta_V \cos 2\theta_V - V_e - V_\nu(\rho_{ee}, \bar{\rho}_{ee})}{\Delta_M(\rho_{ee}, \bar{\rho}_{ee}, \rho_{ex}, \bar{\rho}_{ex})}\right) \ . \tag{29}$$

and a similar expression for antineutrinos. A conservation rule exists relating the diagonal and the off-diagonal density matrix elements that places a further constraint on Eq. (29):

$$[2\,\mathcal{R}e(\rho_{ex})]^2 + [-2\,\mathcal{I}m(\rho_{ex})]^2 + (2\rho_{ee} - 1)^2 = 1 \ . \tag{30}$$

---

[6] In Ref. [32] the conditions were written in neutrino flavor isospin formalism (NFIS) [54]: $s_{x,y} \approx -\alpha \bar{s}_{x,y}$. In addition, the conservation rule $s_x^2 + s_y^2 + s_z^2 = 1/4$ expressed in neutrino flavor isospin (NFIS) formalism translates to $[2\,\mathcal{R}e(\rho_{ex})]^2 + [-2\,\mathcal{I}m(\rho_{ex})]^2 + (2\rho_{ee} - 1)^2 = 1$ in the density matrix formalism utilized in this manuscript (similarly for antineutrinos).

with, again, a similar equation for antineutrinos. If we wish to find a solution to Eq. (29) subject to the conservation rule Eq. (30) we need a third condition. It was suggested in Ref. [54, 55] that adiabatic solutions can be defined as those which have a negligible off-diagonal imaginary component, $\mathcal{I}\mathrm{m}(\rho_{ex})$. Typically during a symmetric MNR transition the off-diagonal imaginary component averages to zero over the entire transition. An example of this can be seen in the bottom panel of Fig. 1. If we require $\mathcal{I}\mathrm{m}(\rho_{ex}) = 0$, and further neglect terms proportional to $\sin 2\theta_V$, a simple closed form analytic expression can be obtained

$$\begin{aligned} P_{\nu_e} \equiv \rho_{ee} &= \frac{1}{2}\left(1 + \frac{\alpha^2 - R^2 - (1-\epsilon)^2}{2R(1-\epsilon)}\right) , \\ P_{\bar{\nu}_e} \equiv \bar{\rho}_{ee} &= \frac{1}{2}\left(1 + \frac{\alpha^2 + R^2 - (1-\epsilon)^2}{2\alpha R}\right) , \end{aligned} \tag{31}$$

with $\epsilon = 2\Delta_V \cos 2\theta_V/(V_e + \Delta_V \cos 2\theta_V)$. In the limit of a large background matter contribution, $V_e \gg \Delta_V$, ϵ can be neglected and these equations reduce to the MNR expressions for the (anti)neutrino survival probabilities obtained by assuming a vanishing separation between the in-medium eigenvalues, Eq. (28). Eqs. (31) are particularly useful when the scales (vaccuum, matter and neutrino potentials) in the problem come close together and the imaginary components of the density matrix can be neglected. We illustrate the usefulness of Eq. (31) in section III F by considering a system where interaction scales are close to each other. In the next section, we will explore the generality of our findings by discussing two distinct systems in which MNR transitions can take place.

D. Discussion of Symmetric and Standard MNR Transitions

In this section we further investigate our MNR conditions described in the previous sections. We consider two scenarios: one that produces a Standard MNR transition as described in Ref. [32], together with the simplest system exhibiting Symmetric MNR motivated by the results presented in Ref. [11] (see Region (III) in Figure 5 of [11]). A characteristic feature of the Symmetric MNR region is that the initial neutrino-neutrino potential starts with a negative sign (antineutrinos dominate close to the neutrino emission) and changes its sign to positive (neutrinos dominate further out) [33]. This is different than the Standard MNR transition region where the neutrino-neutrino potential always remains negative [32].

Therefore, we introduce two models, A and B, that capture the essential features of a Symmetric and a Standard MNR transition, respectively. The parameters of model A were also used in Fig. 1. Repeated here, they are $\mu_\nu = 10\,000\ [\Delta_V]$ and $\alpha(r) = a + br$, with $a = 1.3$ and $b = -0.048$. The matter potential is kept constant at $V_e = 1000\ [\Delta_V]$. For the model B, we use the same parameterization as in [32]: $\mu_\nu(r) = 10\,000\ \mathrm{e}^{-r/10}[\Delta_V]$, $\alpha = 4/3$ and $V_e = 1000\ [\Delta_V]$. In both of these models, r represents distance in units of inverse $|\Delta_V|$. We have defined Δ_V so that it is $+1$ for the normal hierarchy and -1 for the inverted hierarchy. Consistent with available estimates for the placement of MNR in compact object mergers and core collapse supernova accretion disks [11, 33], we have chosen models where $\mu_\nu >> \Delta_V$ throughout the transition.

Model	A	B
Δ_V	± 1	± 1
$V_e\ [\Delta_V]$	1000	1000
$\mu_\nu\ [\Delta_V]$	$10\,000$	$10\,000\ \mathrm{e}^{-r/10}$
α	$1.3 - 0.048\,r$	$4/3$

TABLE I: Chosen parameter values for the Symmetric model (Model A) and the Standard model (Model B): vacuum scale, Δ_V (+1 for normal, -1 for inverted neutrino mass hierarchy), background matter potential, V_e, neutrino-neutrino interaction strength, μ_ν, and the ν_e and $\bar{\nu}_e$ asymmetry factor, α.

In our calculations, we assume neutrinos to be produced as pure flavor states. We follow the evolution of (anti)neutrinos by solving the evolution equations in Eq. (2) with the following initial conditions for the neutrino and antineutrino density matrices in Eq. (3):

$$\rho^0 \equiv \rho(r=0) = \begin{pmatrix} 1 & 0 \\ 0 & 0 \end{pmatrix} = \bar{\rho}(r=0) \equiv \bar{\rho}^0 \ . \tag{32}$$

Taking Eq. (32) and substituting it into Eq. (10) provides information about what V_ν would be in the absence of any oscillation, i.e. $V_\nu^{unosc} = \mu_\nu(1-\alpha)$.

Having set up both models we have one last choice to make which is the vacuum mixing angle. In this section we take the value of the vacuum mixing angle to be consistent with θ_{13}: $\theta_V = 0.15$ [56]. We can now turn to our results, which are presented in Figs. 2 and 3. In the top panels of these figures we show the comparison of analytic and numerical results for the Symmetric (Fig. 2) and Standard (Fig. 3) cases for the inverted and normal hierarchies. In all four top panels, the analytical results match well with the numerical results for the survival probabilities and the transition starts at the resonance location as predicted.

The analytical results were derived from the assumption that the difference between the instantaneous in-medium eigenvalues was close to zero. We verify the appropriateness of this assumption in the middle panels in these figures where we plot the difference of the in-medium mass eigenvalue. We see that this difference, 2 Δ_M, approaches zero. Another prediction, given in Eq. (26), was that the neutrino-neutrino potential V_ν will mirror the matter potential V_e. As can be seen from the bottom panels in these four figures, V_ν deviates strongly from the value it would take on if no oscillation occurred, V_ν^{unosc}, and tracks V_e as expected.

E. Sensitivity to the Vacuum Mixing - Linearized (In)stability Analysis

The models that have been studied in the previous literature (see Ref. [32]), fulfill the MNR conditions outlined in Section III. However, in realistic accretion disk scenarios one expects a variety of conditions that can impact the occurrence of MNR type transitions. According to Eq. (22), which describes the adiabaticity at the location of a resonance, the presence or absence of the resonance transition depends on the interplay of the vacuum parameters and the background density gradients. In previous literature, the measured values for the vacuum mixing parameters have ensured a successful MNR transitions in the considered scenarios. Either reducing the mixing angle or steepening the neutrino and/or matter profiles will shut off the MNR transition. While the vacuum mixing angles are measured, the density gradients of the neutrino and matter profiles in the astrophysical environments are uncertain. The effect of varying density gradients can effectively be mimicked by reducing the vacuum mixing angle. In addition, active-sterile mixing can also induce MNR type transitions. The possible active-sterile mixing angles are currently unknown and their exact values can impact sterile neutrino induced MNR transitions. For simplicity, in this section we illustrate the interplay of the vacuum parameters and the background density gradients by reducing the vacuum mixing angle.

In Figs. 4 and 5 we present the results for our Symmetric (Model A in Table I) and Standard MNR system (Model B) with a reduced vacuum mixing of $\theta_V = 0.001$. It can be seen from the top panels of these two figures that no transition begins at the initial MNR resonance position (first dashed line). From the middle panels, we also see that the difference of the in-medium mass eigenvalues does not hover around zero between the dashed lines, as it would during a MNR transition. Due to the small value of the vacuum mixing, the resonances are non-adiabatic. However, looking again at the top panels, we see that in the inverted hierarchy transitions do take place at other locations. These are self-induced nutation type transitions similar to the type found in core collapse supernovae.

The onset of the self-induced effects has been related to the presence of an instability [18, 39, 40]. In the following, we will apply the linearized stability analysis procedure outlined in Ref. [18] to describe conditions for neutrino flavor instability in systems which have MNR resonances. In order to study the stability of the systems we consider here, it is sufficient to consider the following 2×2 stability matrix (see Appendix):

$$\mathbf{S} = \begin{pmatrix} A_{12} & B_{12} \\ \bar{B}_{21} & \bar{A}_{21} \end{pmatrix} \quad , \tag{33}$$

with

$$\begin{aligned} A_{12} =& H^0_{11} - H^0_{22} + (\rho^0_{22} - \rho^0_{11})\frac{\partial H_{12}}{\partial \rho_{12}} \ , \\ B_{12} =& (\rho^0_{22} - \rho^0_{11})\frac{\partial H_{12}}{\partial \bar{\rho}_{21}} \ , \\ \bar{A}_{21} =& \bar{H}^0_{22} - \bar{H}^0_{11} + (\bar{\rho}^0_{11} - \bar{\rho}^0_{22})\frac{\partial \bar{H}_{21}}{\partial \bar{\rho}_{21}} \ , \\ \bar{B}_{21} =& (\bar{\rho}^0_{11} - \bar{\rho}^0_{22})\frac{\partial \bar{H}_{21}}{\partial \rho_{12}} \ , \end{aligned} \tag{34}$$

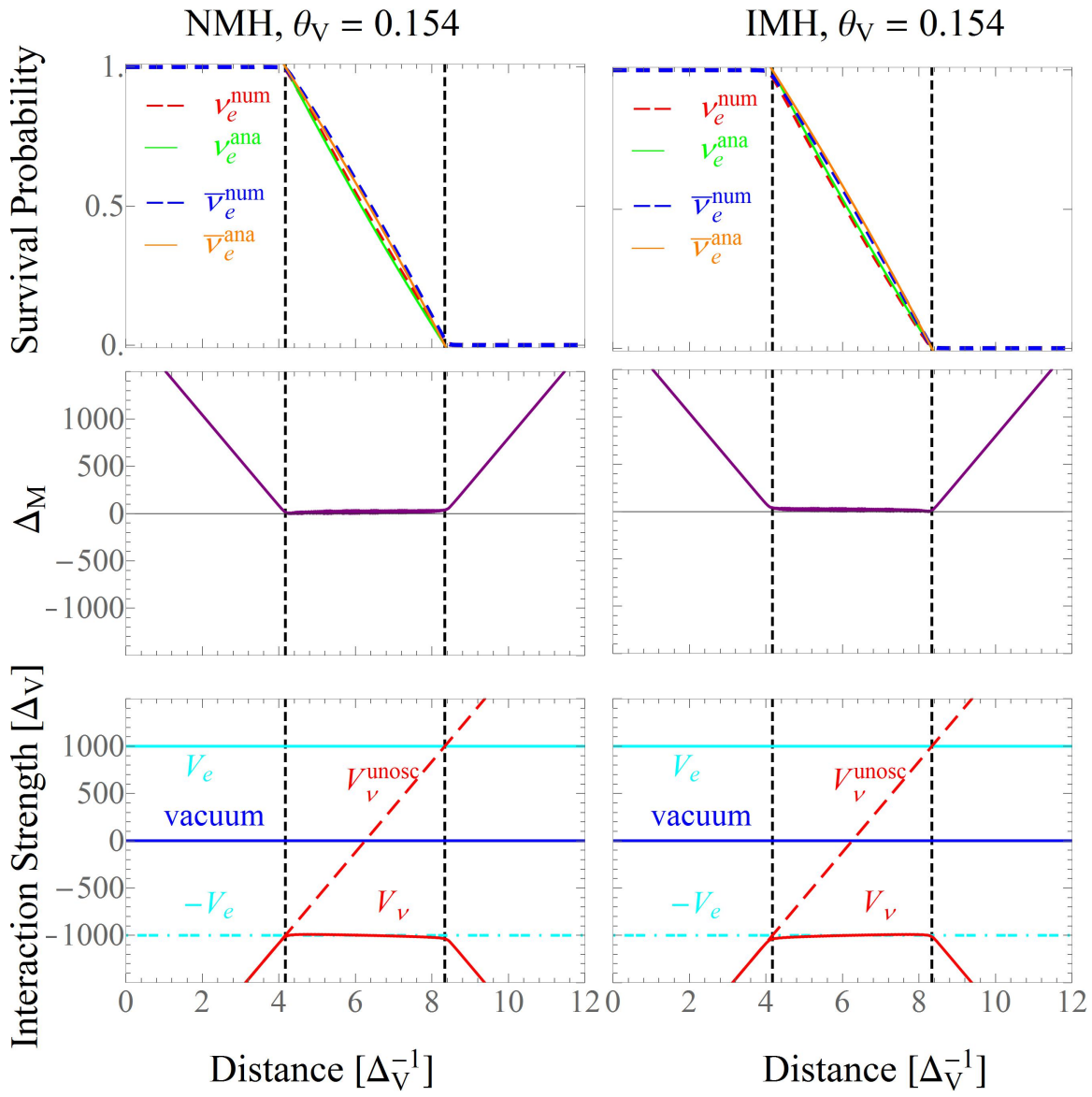

FIG. 2: (Color online) Comparison of numerical results with analytical predictions in the Symmetric MNR model assuming vacuum mixing angle $\theta_V = 0.15$ (model A). Left (right) figures display the results in normal (inverted) mass hierarchy, $\Delta_V = +1(-1)$. **Top figures:** Survival probabilities for ν_e (solid) and $\bar{\nu}_e$ (dashed-dotted lines) with a comparison of numerical results (red) with analytical prediction given by Eq. (28) (green lines). **Middle figures:** Comparison of MNR assumption, $\Delta_M = 0$ (light gray line), with numerically computed in-medium eigenvalue difference (purple line), utilizing Eq. (12) and numerical results for the neutrino and antineutrino densities. **Bottom figures:** Contributions to the total neutrino Hamiltonian, Eq. (9): Vacuum (blue), background matter potential, V_e (cyan), neutrino self interaction potential, V_ν (solid red line) as well as V_ν^{unosc} (dashed red line). During MNR transition, neutrino-neutrino potential actively cancels the background matter contribution and should be compared with $-V_e$. Vertical dashed lines represent the resonance locations according to Eq. (17).

where ρ^0 is given by Eq. (32) and the system is initially described by the Hamiltonian $H^0 = H_M$ with $\rho = \rho^0$, that

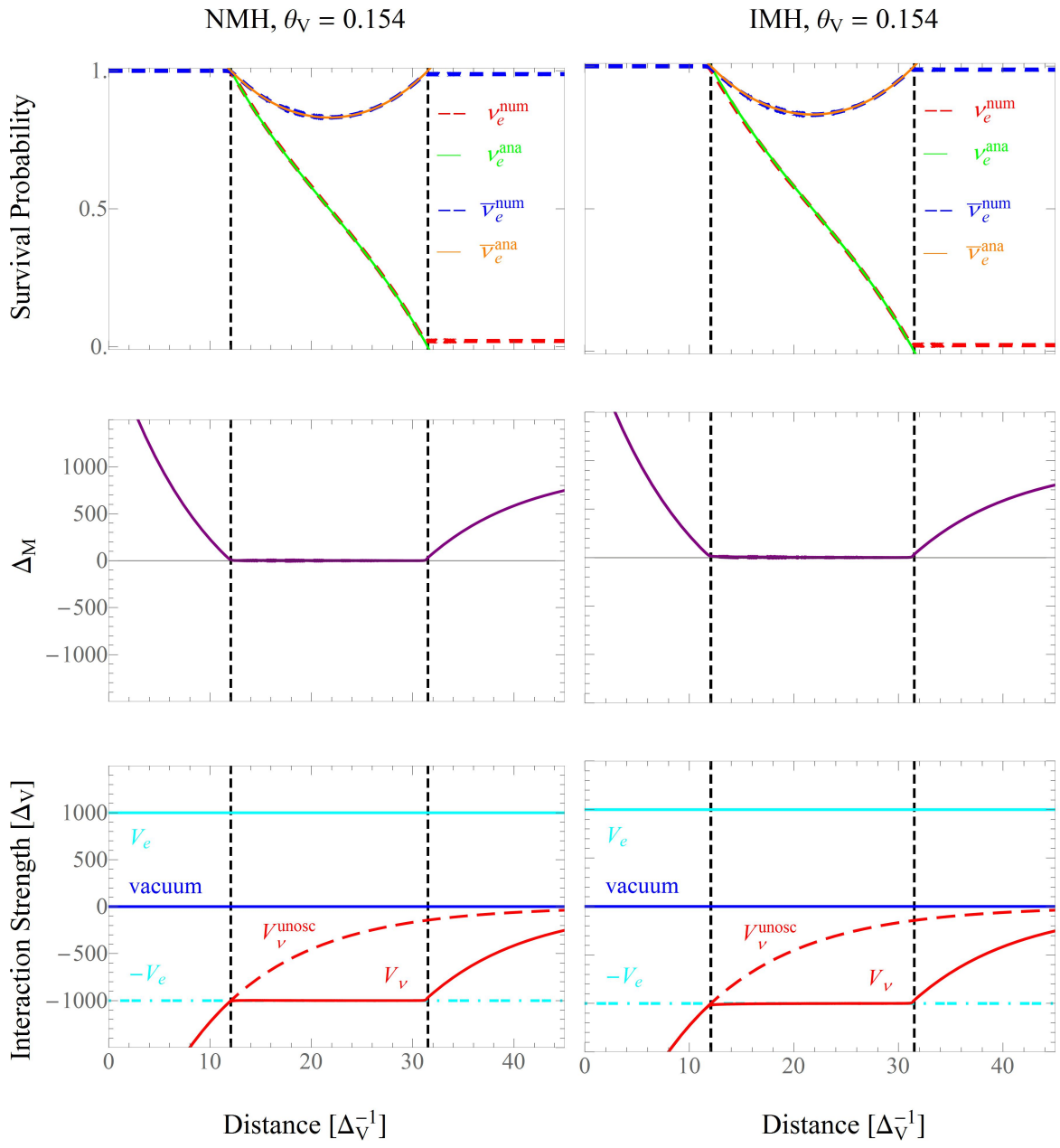

FIG. 3: Comparison of numerical results with analytical predictions in the Standard MNR model (model B) assuming vacuum mixing angle $\theta_V = 0.15$. Lines are as described in Fig. 2.

is, by Eq. (11) with neutrino and antineutrino density matrix elements given according to Eq. (32):

$$\begin{aligned} \overset{(-)}{H}{}^0_{22} - \overset{(-)}{H}{}^0_{11} = \overset{(-)}{\Delta}{}^0_M &= \sqrt{\left(\Delta_V \cos 2\theta_V \overset{(+)}{-} (V_e + \mu_\nu(1-\alpha))\right)^2 + \Delta_V^2 \sin^2 2\theta_V} \ , \\ \frac{\partial H_{12}}{\partial \rho_{12}} = \mu_\nu \ , \quad \frac{\partial H_{12}}{\partial \bar{\rho}_{21}} &= -\mu_\nu \alpha \ , \\ \frac{\partial \bar{H}_{21}}{\partial \rho_{12}} = -\mu_\nu \ , \frac{\partial \bar{H}_{21}}{\partial \bar{\rho}_{21}} &= \mu_\nu \alpha \ . \end{aligned} \tag{35}$$

Then, the elements of the stability matrix become (in the limit $\theta_V \to 0$):

$$\begin{aligned} A_{12} &= -\left(\Delta_V - V_e - \mu_\nu(1-\alpha)\right) - \mu_\nu \ , \\ \bar{A}_{21} &= \left(\Delta_V + V_e + \mu_\nu(1-\alpha)\right) + \alpha\mu_\nu \ , \\ B_{12} &= \alpha\mu_\nu \ , \\ \bar{B}_{21} &= -\mu_\nu \ . \end{aligned} \tag{36}$$

Instability conditions are obtained by solving the eigenvalues, λ, of the stability matrix:

$$|\mathbf{S} - \lambda| = 0 \ . \tag{37}$$

A complex value for the eigenvalue indicates an unstable mode. The stability matrix has eigenvalues

$$\lambda = \frac{1}{2}\left(A_{12} + \bar{A}_{21} \pm \sqrt{(A_{12} - \bar{A}_{21})^2 + 4B_{12}\bar{B}_{21}}\right) \ . \tag{38}$$

The system is unstable if eigenvalues become imaginary, that is, if

$$(A_{12} - \bar{A}_{21})^2 + 4B_{12}\bar{B}_{21} < 0 \ . \tag{39}$$

This stability analysis predicts the conditions under which the system becomes unstable to small perturbations. In the context of self-induced collective effects, the stability analysis gives the conditions for the on-set of self-induced flavor transformations. In the normal mass hierarchy (NMH), eigenvalues of the stability matrix in Eq. (38) are always real. Hence, the system is flavor stable and no flavor transformation occur. In the inverted mass hierarchy (IMH), eigenvalues of the stability matrix become imaginary. The region where the eigenvalues become imaginary for Models A and B is shown as the shaded region in Figs. 4 and 5. The system has an unstable region and exhibits self-induced nutation type transformations in this region.

F. Sensitivity to the Interaction Scales

In this section we provide an example that demonstrates the predictive power of our new analytic expression in Eq. (31) obtained by utilizing the adiabatic assumption, Eq. (24), and neglecting the imaginary component of the off-diagonal density matrix element

In Fig. 6 we have considered the same Symmetric MNR system as described in section III B with reduced neutrino-neutrino interaction strength, $\mu_\nu = 100$ [Δ_V], and matter potential, $V_e = 10$ [Δ_V]. Similarly as in Fig. 1, in the top panel, we illustrate the numerically calculated electron neutrino survival probability and a projected electron neutrino probability associated with the in-medium eigenstate, ν_{1M}, Eq. (24). We can see that the in-medium mass eigenstate tracks the true state of the system over long timescales, as anticipated. In addition, the projected eigenstate solution also better tracks the system over smaller timescales which was not seen in our previous examples where the matter potential was much larger than the vacuum scale. We calculate the adiabaticity parameter, γ in Eq. (18), over both scales and find it to be above 200 for the long (transition) scale and around 50 for the shorter (visible large oscillation) scale, indicating an adiabatic evolution at both scales.

In the bottom panel we also plot the off-diagonal contributions to the density matrix. Again, we find that the off-diagonal imaginary component is nearly zero on average. Therefore, we proceed to use the analytic expression for survival probabilities corrected by the vacuum contribution, Eq. (31), which we plot with dot-dashed line in the top panel. We see that the analytic expression works well on long timescales and correctly predicts the location of resonance conversion to be around 10 [Δ_V^{-1}]. If we were to neglect the vacuum contributions and predict the behavior of the survival probability using Eq. (28), the transition would be expected to take place between 5 [Δ_V^{-1}] and 8 [Δ_V^{-1}]. The analytic expression in Eq. (31), while it accurately predicts the location of the transition, does not do quite as well describing the small scale behavior as does the numerically calculated projection of the in-medium state using Eq. (24). This is because in the analytic prediction the imaginary off-diagonal terms are neglected, and it is these terms that give rise to the oscillations seen in the survival probability.

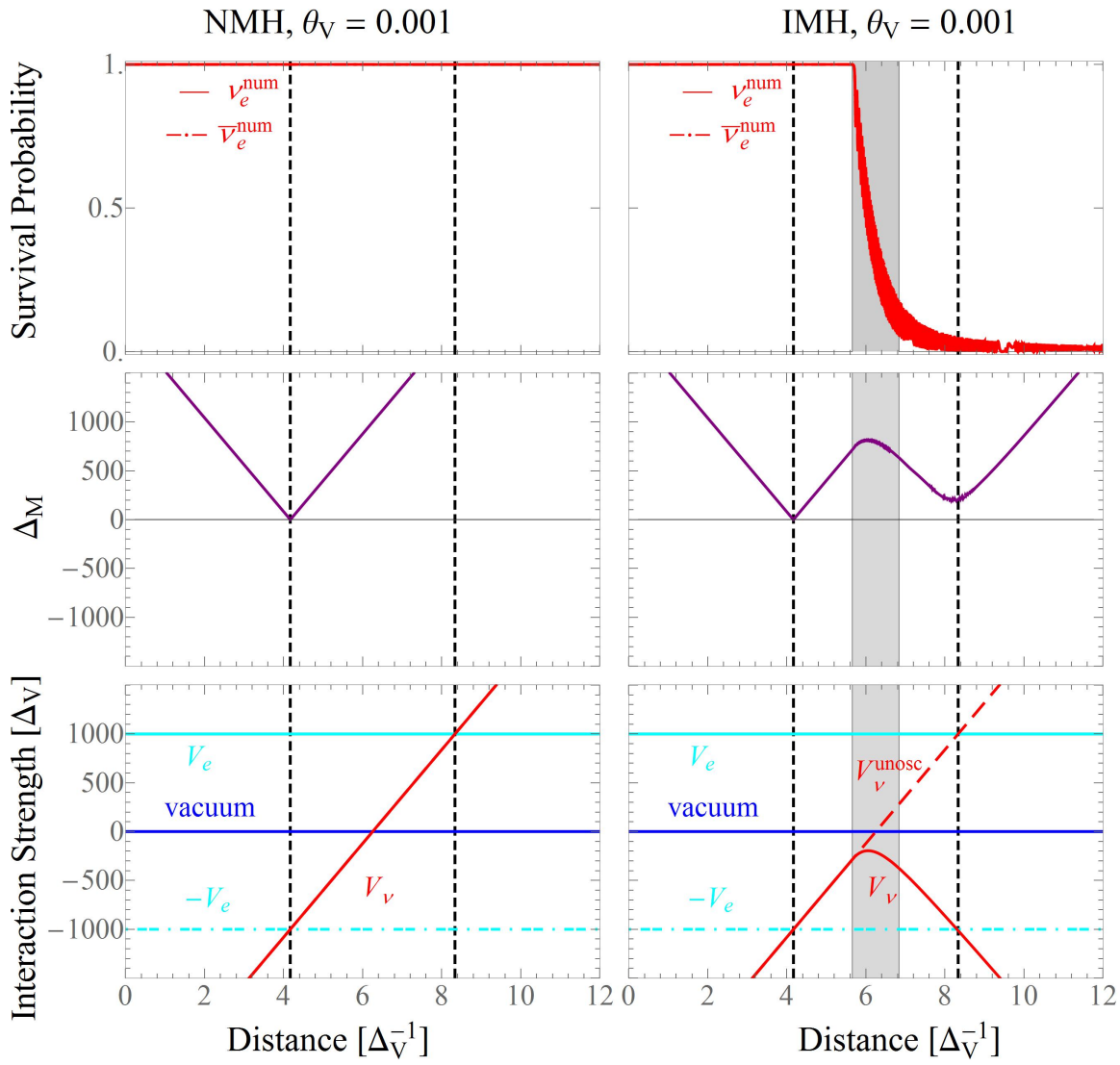

FIG. 4: (Color online) Comparison of numerical results with analytical predictions in the Symmetric model assuming small vacuum mixing angle $\theta_V = 0.001$ (other parameters as in Model A described in Table I). The figure labels and lines plotted are as in Fig. 2. Due to the very small vacuum mixing no flavor transitions take place at the MNR resonance locations (vertical dashed lines). The shaded area represents the instability region according to Eq. (39) (visible only in inverted mass hierarchy (IMH) as the normal mass hierarchy (NMH) is flavor stable, see Section III E for more details). The instability analysis correctly predicts the location of the self-induced nutation type neutrino flavor transitions.

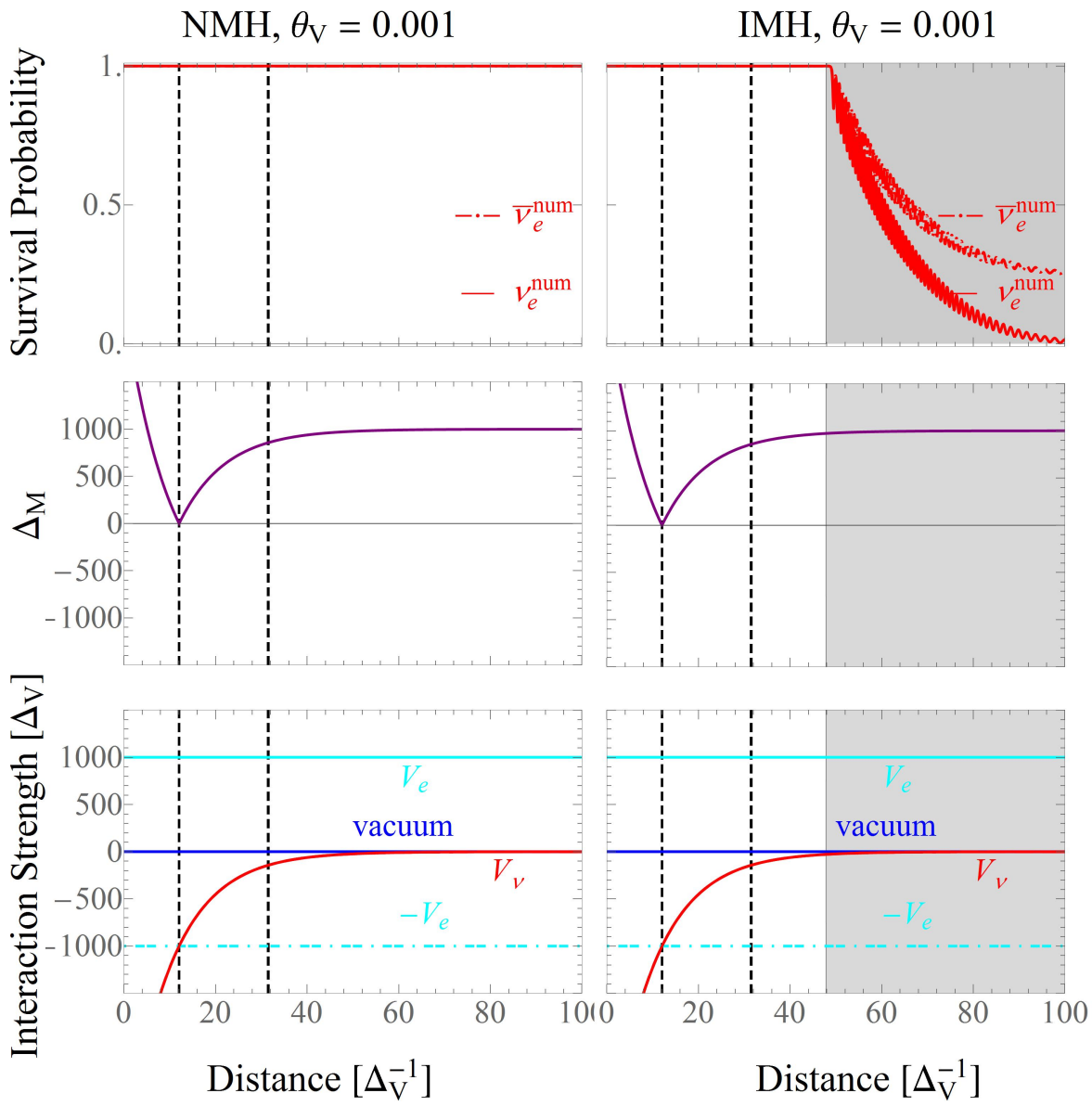

FIG. 5: (Color online) Comparison of numerical results with analytical predictions in the Standard MNR model assuming small vacuum mixing angle $\theta_V = 0.001$ (other parameters as in model B described in Table I). The figure labels and lines are as in Fig. 4. The instability region present in IMH (the shaded area) appears after the MNR region (between vertical dashed lines).

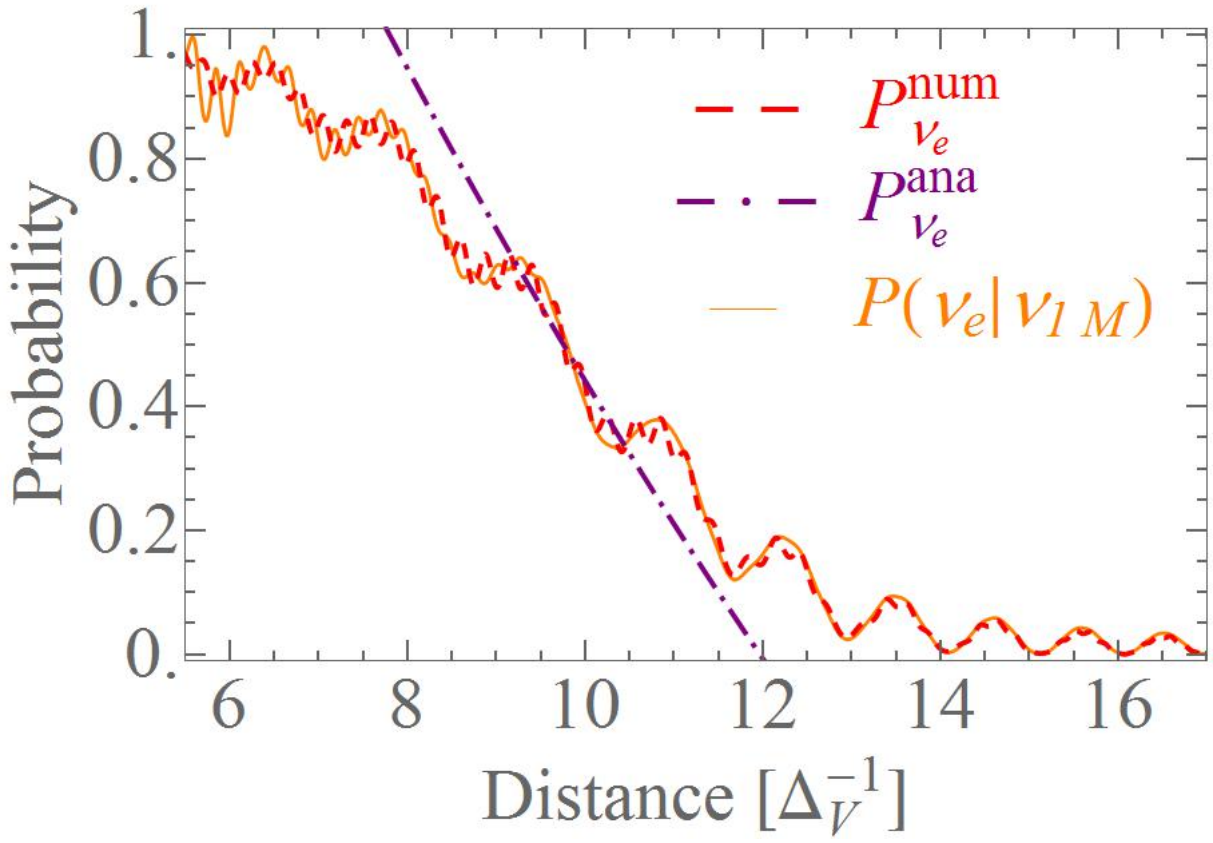

FIG. 6: (Color online) Results for our Symmetric MNR model (see text for details) with interaction strengths $V_e = 10$ and $\mu_\nu = 100$. Top figure: Comparison of numerical calculated ν_e survival probability, P_{ν_e} (red), and probability, $P(\nu_e|\nu_{1M})$ given by Eq. (24) (orange lines) of finding an electron neutrino from in-medium eigenstate, ν_{1M} with analytical prediction given by Eq (31). Bottom figure: real and imaginary components of the off-diagonal neutrino density matrix element.

IV. CONCLUSIONS

In this manuscript we have studied neutrino systems of interest in astrophysical environments, such as compact object mergers, that have the potential to exhibit Matter Neutrino Resonances (MNRs). During MNR transitions the neutrino-neutrino potential actively cancels with the background matter contribution. This can render neutrino flavor transitions at high densities close to the cores of their sources. Therefore, MNRs are of keen interest for nucleosynthesis and also potentially affect the dynamics of the environment.

Using models of monoenergetic neutrino gases, we have provided general resonance conditions applicable to MNR transitions. We have shown that the MNR criteria can be obtained by assuming a small separation of the neutrino in-medium energy eigenstates during the transition. These criteria lead to analytical expressions for neutrino survival probabilities that accurately describe the neutrino flavor evolution during MNR transitions. Furthermore, by assuming an adiabatic evolution, we have derived new analytic expressions for the neutrino survival probabilities that can be applied when the neutrino interaction and the vacuum mixing scales become closer to each other and no evolution occurs in the imaginary off-diagonal density matrix. This offers a powerful tool to predict a location of resonance conversion effects at low background matter potentials when MNR conditions are not fulfilled.

While MNR was originally discussed as a mechanism which leaves neutrinos converted but antineutrinos in their original configuration, we have discussed that MNR transitions can also fully convert both neutrinos and antineutrinos in some cases. Although the final flavor content is different, these symmetric transitions are described in the same way as the standard MNR transitions.

In the systems we have studied, the presence of a MNR transition suppressed the type of self-induced flavor transformation that has been studied in the context of core collapse supernovae. This is because the required initial conditions at the instability point were not met. In order for MNR transitions to take place, the vacuum mixing has to be sufficiently large. In our example models, the measured value of the 'reactor' neutrino mixing angle θ_{13} is sufficient to trigger the MNR transitions. However, smaller angles and/or steeper potentials will suppress these MNR transitions.

If MNR resonances are ineffective, neutrinos can still undergo self-induced flavor transitions. We have applied a general linearization procedure to our Symmetric and Standard MNR models and constructed a stability matrix allowing us to study the flavor stability in these models. In symmetric scenarios, the instability region lies within the MNR resonance region. Thus, if the MNR transition is suppressed, self-induced flavor transition will still occur within the resonance region in the case of the inverted hierarchy. In standard scenarios, the instability region comes after the MNR resonance region.

In an astrophysical system, the exact location of transitions is of significance in determining the impact on dynamical evolution of the environment and conditions for nucleosynthesis. Further investigations are required in order to understand the consequences of neutrinos encountering Matter Neutrino Resonances in more realistic scenarios.

Acknowledgments

We thank J. Kneller and A. Malkus for useful discussions. This work was supported in part by U.S. DOE Grants No. DE-FG02-02ER41216, DE-SC0004786 and DE-SC0006417. During completion of this manuscript another work investigating the underlying physics of the Standard MNR transitions appeared on the arxiv [55].

V. APPENDIX: LINEARIZED (IN)STABILITY ANALYSIS

The (anti)neutrino flavor evolution of our models is described by Eq. (2). Therefore, the evolution of an ij element of the (anti)neutrino density matrix is given by

$$\begin{aligned} \mathrm{i}\frac{\mathrm{d}\rho_{ij}}{\mathrm{d}r} &= \sum_k \left(H_{ik}\rho_{kj} - \rho_{ik}H_{kj}\right) \ , \\ \mathrm{i}\frac{\mathrm{d}\bar{\rho}_{ij}}{\mathrm{d}r} &= \sum_k \left(\bar{H}_{ik}\bar{\rho}_{kj} - \bar{\rho}_{ik}\bar{H}_{kj}\right) \ , \end{aligned} \tag{40}$$

where indices ij refer to the ij element of the corresponding matrix. The above set of evolution equations can be linearized by considering a time dependent small amplitude variation, $\delta\rho$, around the initial configuration, ρ^0, and a

corresponding variation of the density dependent Hamiltonian, δH, around the initial Hamiltonian H^0:

$$\begin{aligned} \rho_{ij} =& \rho^0_{ij} + \delta\rho_{ij} \ , \quad \text{with} \quad \delta\rho_{ij} = \rho'_{ij}\, \mathrm{e}^{-\mathrm{i}\omega r} + \mathrm{H.c.} \quad \text{and} \\ H_{ij} =& H^0_{ij} + \delta H_{ij} \ , \ \text{with} \quad \delta h_{ij} = H'_{ij}\, \mathrm{e}^{-\mathrm{i}\omega r} + \mathrm{H.c.} \ , \end{aligned} \tag{41}$$

where ρ'_{ij}, H'_{ij} are the variation amplitudes and ω describes the variation frequency.

In the case of self-induced collective neutrino effects, the small amplitude variations around the initial configuration, ρ'_{ij} in Eq. (41), are induced by the off-diagonal elements of the (anti)neutrino density matrix. According to our convention, the off-diagonal neutrino Hamiltonian matrix element H_{ij} $(i \neq j)$ depends on the neutrino density matrix element ρ_{ij} and on the antineutrino density matrix element $\bar{\rho}_{ji}$. By retaining only the contributing terms, the variation amplitude of the neutrino Hamiltonian due to the variation of the (anti)neutrino densities can be written as

$$H'_{ij} = \sum_{k<l} \left(\frac{\partial H_{ij}}{\partial \rho_{kl}} \rho'_{kl} + \frac{\partial H_{ij}}{\partial \bar{\rho}_{lk}} \bar{\rho}'_{lk} \right) \ . \tag{42}$$

The initial configuration is described by the in-medium Hamiltonian that is obtained by diagonalizing the flavor basis Hamiltonian at the initial time. Neutrino mixing is modified in-medium as described by Eq. (16). Hence, with large interaction potentials, the in-medium eigenstates initially coincide with flavor states. Therefore, the initial system is described by

$$\left[H^0, \rho^0 \right] = 0 \ , \tag{43}$$

and the initial configuration can be written as

$$\rho^0_{ij} = \rho^0_i \delta_{ij} \ , \quad H^0_{ij} = H^0_i \delta_{ij} \ . \tag{44}$$

Substituting Eqs. (41), (42) and (44) into the evolution equations, Eq. (40), collecting the positive frequency modes, $\mathrm{e}^{-\mathrm{i}\omega r}$ $(i < j)$, and neglecting the higher-order corrections from $[\delta h, \delta\rho]$, one obtains the following eigenvalue equations

$$\begin{aligned} \omega \rho'_{ij} =& \sum_{k<l} \left\{ \left[(H^0_k - H^0_l)\delta_{ik}\delta_{jl} + (\rho^0_j - \rho^0_i) \frac{\partial H_{ij}}{\partial \rho_{kl}} \right] \rho'_{kl} + (\rho^0_j - \rho^0_i) \frac{\partial H_{ij}}{\partial \bar{\rho}_{lk}} \bar{\rho}'_{lk} \right\} \ , \\ \omega \bar{\rho}'_{ji} =& \sum_{k<l} \left\{ \left[(\bar{H}^0_l - H^0_l)\delta_{il}\delta_{jk} + (\bar{\rho}^0_i - \rho^0_j) \frac{\partial \bar{H}_{ji}}{\partial \bar{\rho}_{lk}} \right] \bar{\rho}'_{lk} + (\bar{\rho}^0_i - \rho^0_j) \frac{\partial \bar{H}_{ji}}{\partial \rho_{kl}} \rho'_{kl} \right\} \ , \end{aligned} \tag{45}$$

with eigenvalues ω and eigenvectors $\overset{(-)}{\rho}{}'$. There exist two sets of eigenvalue equations, one for ω and another one for its complex conjugate which can be obtained by collecting the $\mathrm{e}^{+\mathrm{i}\omega^* r}$ modes.

If the eigenvalues $\omega \in \mathcal{R}e$, system has a stable solution with collective oscillation modes

$$\rho_{ij} = 2\rho'_{ij} \cos\omega_s r \ . \tag{46}$$

where ω_s represents the *synchronized* oscillation frequency with oscillation amplitude $2\rho'_{ij}$. On the other hand, if $\omega \in \mathcal{I}m$, the variations can grow exponentially, indicating that the system has become unstable and the linearized equations no longer serve as a good approximation. In the context of self-induced collective neutrino effects, instability indicates the on-set of the nutation type (or *bipolar*) oscillations.

The linearized eigenvalue equations, Eqs. (45), can be written in a compact matrix form by introducing *Stability matrix*, $\mathbf{S}$:

$$\omega \begin{pmatrix} \rho' \\ \bar{\rho}' \end{pmatrix} = \mathbf{S} \begin{pmatrix} \rho' \\ \bar{\rho}' \end{pmatrix} \ , \tag{47}$$

where

$$\mathbf{S} = \begin{pmatrix} A & B \\ \bar{B} & \bar{A} \end{pmatrix} \quad , \tag{48}$$

with elements

$$
\begin{aligned}
A_{ij,kl} &= (H^0_k - H^0_l)\delta_{ik}\delta_{jl} + (\rho^0_j - \rho^0_i)\frac{\partial H_{ij}}{\partial \rho_{kl}} \ , \\
\bar{A}_{ij,kl} &= (\bar{H}^0_l - H^0_l)\delta_{il}\delta_{jk} + (\rho^0_i - \rho^0_j)\frac{\partial \bar{H}_{ji}}{\partial \bar{\rho}_{lk}} \ , \\
B_{ij,kl} &= (\rho^0_j - \rho^0_i)\frac{\partial H_{ij}}{\partial \bar{\rho}_{lk}} \ , \\
\bar{B}_{ij,kl} &= (\bar{\rho}^0_i - \rho^0_j)\frac{\partial \bar{H}_{ji}}{\partial \rho_{kl}} \ .
\end{aligned}
\tag{49}
$$

$\overset{(-)}{A}, \overset{(-)}{B}$ are $N \times N$ matrices with $N = 0.5\, n_f \times (n_f - 1) \times n_E \times n_u \times n_{ini}$ where n_f, n_E, n_u, n_{ini} are the number of neutrino families, neutrino energies, angular modes and initial conditions, respectively, while ρ' and $\bar{\rho}$ are in turn N-dimensional vectors of variation amplitudes.

Instability conditions are obtained by studying the eigenvalues of the stability matrix as discussed in Section III E. In case of two (anti)neutrino flavors with single energy and emission angle, the system can be decomposed into two subsystems described by a subsystem with $(1, 2)$ element of the neutrino density matrix linked to $(2, 1)$ element of the antineutrino density matrix and another subsystem described by the complex conjugates of the corresponding elements. The two subsystems have identical stability conditions. This consideration leads to the form of the stability matrix as shown in Eq. (33).

[1] C. Palenzuela, S. Liebling, D. Neilsen, L. Lehner, O. Caballero, et al. (2015), 1505.01607.
[2] L. Dessart, C. Ott, A. Burrows, S. Rosswog, and E. Livne, Astrophys.J. **690**, 1681 (2009), 0806.4380.
[3] M. B. Deaton, M. D. Duez, F. Foucart, E. O'Connor, C. D. Ott, et al., Astrophys.J. **776**, 47 (2013), 1304.3384.
[4] A. Perego, S. Rosswog, R. Cabezon, O. Korobkin, R. Kaeppeli, et al. (2014), 1405.6730.
[5] E. O'Connor, Astrophys. J. Suppl. **219**, 24 (2015), 1411.7058.
[6] E. Abdikamalov, A. Burrows, C. D. Ott, F. Loffler, E. O'Connor, J. C. Dolence, and E. Schnetter, Astrophys. J. **755**, 111 (2012), 1203.2915.
[7] I. Tamborra, G. Raffelt, F. Hanke, H.-T. Janka, and B. Mueller, Phys. Rev. **D90**, 045032 (2014), 1406.0006.
[8] R. Surman, G. C. McLaughlin, and W. R. Hix, Astrophys. J. **643**, 1057 (2006), astro-ph/0509365.
[9] L. Roberts, S. Woosley, and R. Hoffman, Astrophys.J. **722**, 954 (2010), 1004.4916.
[10] H. Duan, A. Friedland, G. C. McLaughlin, and R. Surman, J. Phys. **G38**, 035201 (2011), 1012.0532.
[11] A. Malkus, J. P. Kneller, G. C. McLaughlin, and R. Surman, Phys. Rev. **D86**, 085015 (2012), 1207.6648.
[12] G. Sigl and G. Raffelt, Nucl. Phys. **B406**, 423 (1993).
[13] A. B. Balantekin and Y. Pehlivan, J. Phys. **G34**, 47 (2007), astro-ph/0607527.
[14] A. Friedland, B. H. J. McKellar, and I. Okuniewicz, Phys. Rev. **D73**, 093002 (2006), hep-ph/0602016.
[15] C. Y. Cardall, Phys. Rev. **D78**, 085017 (2008), 0712.1188.
[16] C. Fidler, M. Herranen, K. Kainulainen, and P. M. Rahkila, JHEP **02**, 065 (2012), 1108.2309.
[17] C. Volpe, D. Vaananen, and C. Espinoza, Phys. Rev. **D87**, 113010 (2013), 1302.2374.
[18] D. Vaananen and C. Volpe, Phys. Rev. **D88**, 065003 (2013), 1306.6372.
[19] A. Vlasenko, G. M. Fuller, and V. Cirigliano, Phys. Rev. **D89**, 105004 (2014), 1309.2628.
[20] J. Serreau and C. Volpe, Phys. Rev. **D90**, 125040 (2014), 1409.3591.
[21] L. Wolfenstein, Phys. Rev. D **17**, 2369 (1978).
[22] S. P. Mikheyev and A. Y. Smirnov, Yadernaya Fizika **42**, 1441 (1985).
[23] Q. R. Ahmad et al. (SNO), Phys. Rev. Lett. **89**, 011301 (2002), nucl-ex/0204008.
[24] K. Eguchi et al. (KamLAND Collaboration), Phys.Rev.Lett. **90**, 021802 (2003), hep-ex/0212021.
[25] H. Duan and J. P. Kneller, J. Phys. **G36**, 113201 (2009), 0904.0974.
[26] H. Duan, G. M. Fuller, and Y.-Z. Qian, Ann. Rev. Nucl. Part. Sci. **60**, 569 (2010), 1001.2799.
[27] H. Duan and A. Friedland, Phys.Rev.Lett. **106**, 091101 (2011), 1006.2359.
[28] J. F. Cherry, J. Carlson, A. Friedland, G. M. Fuller, and A. Vlasenko, Phys. Rev. **D87**, 085037 (2013), 1302.1159.
[29] A. Vlasenko, G. M. Fuller, and V. Cirigliano (2014), 1406.6724.
[30] V. Cirigliano, G. M. Fuller, and A. Vlasenko, Phys. Lett. **B747**, 27 (2015), 1406.5558.
[31] A. Kartavtsev, G. Raffelt, and H. Vogel, Phys. Rev. **D91**, 125020 (2015), 1504.03230.
[32] A. Malkus, A. Friedland, and G. C. McLaughlin (2014), 1403.5797.
[33] A. Malkus, G. C. McLaughlin, and R. Surman (2015), 1507.00946.
[34] S. Hannestad, G. G. Raffelt, G. Sigl, and Y. Y. Wong, Phys.Rev. **D74**, 105010 (2006), astro-ph/0608695.

[35] G. G. Raffelt and A. Y. Smirnov, Phys.Rev. **D76**, 125008 (2007), 0709.4641.
[36] B. Dasgupta and A. Dighe, Phys. Rev. **D77**, 113002 (2008), 0712.3798.
[37] S. Galais, J. Kneller, and C. Volpe, J. Phys. **G39**, 035201 (2012), 1102.1471.
[38] Y. Pehlivan, A. B. Balantekin, T. Kajino, and T. Yoshida, Phys. Rev. **D84**, 065008 (2011), 1105.1182.
[39] R. Sawyer, Phys.Rev. **D79**, 105003 (2009), 0803.4319.
[40] A. Banerjee, A. Dighe, and G. Raffelt, Phys.Rev. **D84**, 053013 (2011), 1107.2308.
[41] S. Sarikas, G. G. Raffelt, L. Hudepohl, and H.-T. Janka, Phys.Rev.Lett. **108**, 061101 (2012), 1109.3601.
[42] N. Saviano, S. Chakraborty, T. Fischer, and A. Mirizzi, Phys.Rev. **D85**, 113002 (2012), 1203.1484.
[43] A. Mirizzi and P. D. Serpico, Phys.Rev.Lett. **108**, 231102 (2012), 1110.0022.
[44] A. Mirizzi and P. D. Serpico, Phys.Rev. **D86**, 085010 (2012), 1208.0157.
[45] R. F. Sawyer (2015), 1509.03323.
[46] S. Sarikas, D. d. S. Seixas, and G. Raffelt, Phys.Rev. **D86**, 125020 (2012), 1210.4557.
[47] S. Sarikas, I. Tamborra, G. Raffelt, L. Hudepohl, and H.-T. Janka, Phys.Rev. **D85**, 113007 (2012), 1204.0971.
[48] H. Duan, Phys. Rev. **D88**, 125008 (2013), 1309.7377.
[49] G. Raffelt, S. Sarikas, and D. d. S. Seixas (2013), 1305.7140.
[50] S. Chakraborty, G. Raffelt, H.-T. Janka, and B. Mueller (2014), 1412.0670.
[51] B. Dasgupta and A. Mirizzi (2015), 1509.03171.
[52] S. Chakraborty, R. S. Hansen, I. Izaguirre, and G. Raffelt (2015), 1507.07569.
[53] C. Giunti, J. Phys. **G34**, R93 (2007), hep-ph/0608070.
[54] H. Duan, G. M. Fuller, and Y.-Z. Qian, Phys. Rev. **D74**, 123004 (2006), astro-ph/0511275.
[55] M.-R. Wu, H. Duan, and Y.-Z. Qian (2015), 1509.08975.
[56] K. A. Olive et al. (Particle Data Group), Chin. Phys. **C38**, 090001 (2014).